Appl. Math. Mech. -Engl. Ed., **38**(1), 125–136 (2017)
DOI 10.1007/s10483-017-2155-6

Applied Mathematics and Mechanics (English Edition)

Heat transfer of nanofluids considering nanoparticle migration and second-order slip velocity*

Jing ZHU[1,†], Shengnan WANG[1], Liancun ZHENG[1], Xinxin ZHANG[2]

1. Department of Applied Mathematics, University of Science and Technology Beijing, Beijing 100083, China;
2. Department of Mechanical Engineering, University of Science and Technology Beijing, Beijing 100083, China

Abstract The heat transfer of a magnetohydrodynamics nanofluid inside an annulus considering the second-order slip condition and nanoparticle migration is theoretically investigated. A second-order slip condition, which appropriately represents the non-equilibrium region near the interface, is prescribed rather than the no-slip condition and the linear Navier slip condition. To impose different temperature gradients, the outer wall is subjected to q_2, the inner wall is subjected to q_1, and $q_1 > q_2$. A modified two-component four-equation non-homogeneous equilibrium model is employed for the nanofluid, which have been reduced to two-point ordinary boundary value differential equations in the consideration of the thermally and hydrodynamically fully developed flow. The homotopy analysis method (HAM) is employed to solve the equations, and the h-curves are plotted to verify the accuracy and efficiency of the solutions. Moreover, the effects of the physical factors on the flow and heat transfer are discussed in detail, and the semi-analytical relation between Nu_{B} and N_{BT} is obtained.

Key words nanofluid, second-order slip, nanoparticle migration, homotopy analysis method (HAM), semi-analytical relation

Chinese Library Classification O241.81
2010 Mathematics Subject Classification 34A25, 76D10, 80A20

Nomenclature

B_0,	magnetic field strength;	C_{htc},	dimensionless heat transfer coefficient;
C_p,	specific heat ($\mathrm{m}^2 \cdot \mathrm{s}^{-2} \cdot \mathrm{K}^{-1}$);	λ_1, λ_2,	slip parameters of the velocity;
q_{w},	surface heat flux;	ρ,	density ($\mathrm{g{\cdot}m^{-3}}$).
N_{p},	non-dimensional pressure drop;	R,	radius (m);
Nu,	Nusselt number;	p,	pressure (Pa);
Ha,	Hartmann number;	U,	axial velocity ($\mathrm{m{\cdot}s^{-1}}$);
ϕ,	nanoparticle volume fraction;	η,	transverse direction;
N_{BT},	ratio of the Brownian to thermophoretic diffusivities;	σ,	electrical conductivity;

* Received Mar. 15, 2016 / Revised Jun. 8, 2016
Project supported by the National Natural Science Foundation of China (Nos. 51476191 and 51406008)
† Corresponding author, E-mail: zhujing@ustb.edu.cn

μ, dynamic viscosity ($\mathrm{kg \cdot m^{-1} \cdot s^{-1}}$);
k, thermal conductivity ($\mathrm{W \cdot m^{-1} \cdot K^{-1}}$);
h, heat transfer coefficient ($\mathrm{W \cdot m^{-2} \cdot K^{-1}}$);
γ, ratio of the temperature difference between the wall and the fluid to the absolute temperature.

1 Introduction

Nowadays, the study on the heat transfer and nanofluid flow inside a annular pipe has been a topic of great interest. Nanofluids are significant for the production of nanostructured materials, whose sizes are below 100 nm, the engineering of complex fluids, and the cleaning oil from solid surfaces[1] owing to their excellent wetting and spreading behaviors. Heat transfer is very important in the high-temperature processes like gas turbines, nuclear plants, thermal energy storage, etc. Some researchers[2–4] have investigated the effects of the slip condition in nanofluids via molecular dynamics simulations.

The slip degree at the boundary depends on a number of interfacial parameters, including the strength of the thermal roughness of the interface, the liquid-solid coupling, and the liquid densities[5]. A second-order slip condition, which appropriately represents the non-equilibrium region near the interface, is prescribed rather than the no-slip condition and the linear Navier slip condition. First, the conventional no-slip boundary conditions at the walls may not be accurate when the dimensions are reduced to microscale. Secondly, the linear Navier slip condition performs well when it is at a sufficiently low shear rate. However, at higher shear rates, when the slip length increases rapidly, the Navier slip condition will break down. Therefore, many researchers[6–7] proposed the nonlinear slip conditions. Thirdly, due to the comparison between the calculation results and the experimental data, the values calculated by the second-order slip boundary condition are more close to the experimental data[8]. Therefore, many scholars investigated the effects of the velocity slip condition on the flow and heat transfer with Nu_{B}. Zhu et al.[9] studied the effects of the second-order velocity slip and nanoparticle migration on the Buongiorno nanofluid flow.

Originally, the proposed models are twofold, i.e., homogeneous flow models and dispersion models. In 2006, Buongiorno[10] certified that homogeneous models were more suitable to predict the nanofluid heat transfer coefficient. Simultaneously, the dispersion effect was completely negligible due to the nanoparticle size. Therefore, he proposed a two-component four equation non-homogeneous equilibrium model for the convective transport in nanofluids. On the basis of this model, Sheikholeslami et al.[11] studied the forced convection heat transfer in a semi-annulus under the influence of a variable magnetic field. Kasaeipoor et al.[12] studied the convection of the Cu-water nanofluid in a vented T-shaped cavity in the presence of magnetic field.

Till now, a number of works have been studied on the fluid flow and heat transfer with asymmetric heating inside a annular pipe[13–14]. However, very limited investigation has been given to the the heat transfer of nanofluids considering the nanoparticle migration under high-order slip boundary conditions, and there is no attention on the analytic solution. Hence, in the current research, a theoretical study of fully developed convection heat transfer of the nanofluid with a uniform magnetic field inside a annular pipe is presented based on the modified Buongiorno model[10]. It is of particular interest to study the effects of a second-order slip condition and N_{BT} on the hydrodynamic and thermal characteristics of the system. The analytical approximations of the solutions are derived by the homotopy analysis method (HAM). The residual error curves and h-curves are verified to the accuracy and efficiency for the HAM solutions. Furthermore, the semi-analytical relation between Nu_{B} and N_{BT} are obtained.

2 Mathematical analysis

Consider an magnetohydrodynamics, laminar, and two-dimensional flow of a nanofluid inside a annular pipe with the second-order slip condition, which is subjected to different heat fluxes at the outer wall q_2 and the inner wall q_1 such that $q_1 > q_2$. A two-dimensional coordinate frame is selected, where the x-axis is aligned parallel and the r-axis is normal to the walls. A modified two-component heterogeneous model is employed for the nanofluid. Consequently, the basic incompressible conservation equations of the mass, momentum, thermal energy, and nanoparticle fraction can be expressed as follows:

$$\frac{\partial \rho U_i}{\partial x_i} = 0, \tag{1}$$

$$\frac{\partial \rho U_i U_j}{\partial x_i} + \frac{\partial \rho U_i}{\partial t} = -\frac{\partial p}{\partial x_i} + \frac{\partial}{\partial x_i}\mu\Big(\frac{\partial U_i}{\partial x_i} + \frac{\partial U_j}{\partial x_j}\Big) - \sigma B_0^2 U_i, \tag{2}$$

$$\frac{\partial \rho C_p U_i T}{\partial x_i} + \frac{\partial \rho C_p T}{\partial t} = \frac{\partial}{\partial x_i}\Big(k\frac{\partial T}{\partial x_i}\Big) + \rho_{\mathrm{p}} C_{\mathrm{pp}}\Big(D_{\mathrm{B}}\frac{\partial \phi}{\partial x_i} + \frac{D_{\mathrm{T}}}{T}\frac{\partial T}{\partial x_i}\Big)\frac{\partial T}{\partial x_i}, \tag{3}$$

$$\frac{\partial U_i \phi}{\partial x_i} + \frac{\partial \phi}{\partial t} = \frac{\partial}{\partial x_i}\Big(D_{\mathrm{B}}\frac{\partial \phi}{\partial x_i} + \frac{D_{\mathrm{T}}}{T}\frac{\partial T}{\partial x_i}\Big), \tag{4}$$

where U_i represents the velocity components, T is the local temperature, p is the pressure, σ is the electric conductivity, B_0 is the uniform magnetic field strength, and D_{B} and D_{T} are the Brownian diffusion and the thermophoretic diffusion coefficients, respectively. ρ, μ, k, and C_p, depending on the nanoparticle volume fractions, are the density, the dynamic viscosity, the thermal conductivity, and the specific heat capacity of the nanofluid, respectively. The relations of Buongiorno[10], which correlate the viscosity and the thermal conductivity of the nanofluid based on the experimental data of Pak and Cho[15], are used. The expressions are

$$\mu(\phi) = \begin{cases} \mu_{\mathrm{bf}}(1 + 39.11\phi + 533.9\phi^2) & (\text{Al-water}), \\ \mu_{\mathrm{bf}}(1 + 5.45\phi + 108.2\phi^2) & (\text{TiO}_2\text{-water}), \end{cases} \tag{5}$$

$$k(\phi) = \begin{cases} k_{\mathrm{bf}}(1 + 7.47\phi) & (\text{Al-water}), \\ k_{\mathrm{bf}}(1 + 2.92\phi - 11.99\phi^2) & (\text{TiO}_2\text{-water}), \end{cases} \tag{6}$$

$$\begin{cases} \rho = \phi\rho_{\mathrm{p}} + (1-\phi)\rho_{\mathrm{bf}}, \\ C_p = \dfrac{\phi\rho_{\mathrm{p}} C_{\mathrm{pp}} + (1-\phi)\rho_{\mathrm{bf}} C_{p\mathrm{bf}}}{\rho}, \end{cases} \tag{7}$$

where bf stands for the base fluid, and p stands for the particle. The thermophysical properties of Al and TiO_2 nanoparticles and the base fluid-water are provided as follows:

$$\begin{cases} C_{p_{\mathrm{bf}}} = 4\ 182\ \mathrm{J \cdot kg^{-1}} \cdot K^{-1}, \quad k_{\mathrm{bf}} = 0.597\ \mathrm{W} \cdot m^{-1} \cdot k^{-1}, \\ \rho_{\mathrm{bf}} = 998.2\ \mathrm{kg} \cdot m^{-3}, \quad \mu_{\mathrm{bf}} = 9.93 \times 10^{-4}\ \mathrm{kg \cdot m^{-1} \cdot s^{-1}}, \\ C_{p\mathrm{Al}} = 773\ \mathrm{J \cdot kg^{-1} \cdot K^{-1}}, \quad k_{\mathrm{Al}} = 36\ \mathrm{W \cdot m^{-1} \cdot k^{-1}}, \\ \rho_{\mathrm{Al}} = 3\ 380\ \mathrm{kg} \cdot m^{-3}, \quad C_{p\mathrm{TiO_2}} = 4\ 182\ \mathrm{J \cdot kg^{-1} \cdot K^{-1}}, \\ k_{\mathrm{TiO_2}} = 8.4\ \mathrm{W \cdot m^{-1} \cdot k^{-1}}, \quad \rho_{\mathrm{TiO_2}} = 4\ 175\ \mathrm{kg \cdot m^{-3}}. \end{cases}$$

Assuming the hydrodynamically and thermally fully developed conditions, Eqs. (1)–(4) can be simply reduced, i.e.,

$$-\frac{\mathrm{d}p}{\mathrm{d}x}+\frac{1}{r}\frac{\partial}{\partial r}\Big(r\mu(\phi)\frac{\partial U}{\partial r}\Big)-\sigma B_0^2 u=0, \tag{8}$$

$$\rho C_p U\frac{\partial T}{\partial x}-\frac{1}{r}\frac{\partial}{\partial r}\Big(rk(\phi)\frac{\partial T}{\partial r}\Big)-Q_0(T-T_{\mathrm{w}})+\frac{\partial q_{\mathrm{r}}}{\partial r}=0, \tag{9}$$

$$\frac{1}{r}\frac{\partial}{\partial r}\Big(D_{\mathrm{B}}T\frac{\partial \phi}{\partial r}+\frac{D_{\mathrm{T}}}{T}\frac{\partial T}{\partial r}\Big)=0. \tag{10}$$

The boundary conditions for this problem can be expressed as follows:

$$r=0:\ \frac{\partial U}{\partial r}=0,\quad k_{\mathrm{tw}}\frac{\partial T}{\partial r}=q_1,\quad \frac{\partial \phi}{\partial r}=-\frac{D_{\mathrm{T}}}{D_{\mathrm{B}}}\frac{1}{T}\frac{\partial T}{\partial r}, \tag{11}$$

$$r=R_2-R_1:\ U=\lambda_1\frac{\partial U}{\partial r}+\lambda_2\frac{\partial^2 U}{\partial r^2},\quad k_{\mathrm{tw}}\frac{\partial T}{\partial r}=q_2,\quad \frac{\partial \phi}{\partial r}=-\frac{D_{\mathrm{T}}}{D_{\mathrm{B}}}\frac{1}{T}\frac{\partial T}{\partial r}. \tag{12}$$

Regarding the nanoparticle continuity equation, it is obvious that the Brownian diffusion flux and the thermophoretic diffusion flux are cancelled out everywhere. Introduce the following non-dimensional parameters:

$$\begin{cases}\eta=\dfrac{R_2-R_1-r}{R_2-R_1},\quad u=\dfrac{U\mu_{\mathrm{w}}}{-(\mathrm{d}p/\mathrm{d}x)(R_2-R_1)^2},\\[2ex] \theta=\dfrac{D_{\mathrm{B}}}{D_{\mathrm{T}}}\dfrac{k_{\mathrm{tw}}(T-T_{\mathrm{w}})}{q_{\mathrm{tw}}(R_2-R_1)}\quad Ha^2=\dfrac{\sigma B_0^2(R_2-R_1)^2}{\mu_{\mathrm{w}}},\\[2ex] N_{\mathrm{BT}}=\dfrac{k_{\mathrm{tw}}t_{\mathrm{tw}}^2}{q_{\mathrm{tw}}(R_2-R_1)},\quad \gamma=\dfrac{q_{\mathrm{w}}(R_2-R_1)}{k_{\mathrm{w}}T_{\mathrm{w}}}.\end{cases} \tag{13}$$

The radiative heat flux q_{r} is described by the Rosseland approximation[16] such that

$$q_{\mathrm{r}}=-\frac{4\sigma^*}{3\delta}\frac{\partial T^4}{\partial r^4}, \tag{14}$$

where σ^* and δ are the Stefan-Boltzmann constant and the mean absorption coefficient, respectively. We assume that the temperature differences within the flow are sufficiently small so that T^4 can be expressed as a linear function after using the Taylor series to expand T^4 about the free stream temperature T_∞ and neglecting the higher-order terms. The result is

$$T^4\cong 4T_\infty^3 T-3T_\infty^4. \tag{15}$$

Equations (8)–(10) can be reduced to

$$(1-\eta)\Big(\frac{\mathrm{d}^2u}{\mathrm{d}\eta^2}\mu(\phi)+\frac{\mathrm{d}\mu(\phi)}{\mathrm{d}\eta}\frac{\mathrm{d}u}{\mathrm{d}\eta}+\mu_{\mathrm{w}}(1-Ha^2)u\Big)-\frac{\mathrm{d}u}{\mathrm{d}\eta}\mu(\phi)=0, \tag{16}$$

$$\begin{aligned}&(1-\eta)\Big(\frac{\mathrm{d}^2\theta}{\mathrm{d}\eta^2}k(\phi)+\frac{\mathrm{d}k(\phi)}{\mathrm{d}\eta}\frac{\mathrm{d}\theta}{\mathrm{d}\eta}-2(1+\epsilon)\frac{k_{\mathrm{w}}}{q_{\mathrm{w}}}\frac{\rho cu}{\langle\rho cu\rangle}\\&+Q_0\theta(1-\zeta)^2+\frac{16\sigma^*}{3k^*}\frac{\mathrm{d}^2\theta}{\mathrm{d}\eta^2}\Big)-\frac{\mathrm{d}\theta}{\mathrm{d}\eta}k(\phi)=0,\end{aligned} \tag{17}$$

$$N_{\mathrm{BT}}(1+\gamma\theta)^2\frac{\partial\phi}{\partial\eta}-\phi\frac{\partial\theta}{\partial\eta}=0. \tag{18}$$

The boundary conditions are

$$\eta = 0: \ u = \lambda_1 \frac{\partial u}{\partial \eta} \frac{1}{R_2 - R_1} + \lambda_2 \frac{\partial^2 u}{\partial \eta^2} \frac{1}{(R_2 - R_1)^2}, \quad \frac{\partial \theta}{\partial \eta} = -1, \quad \theta = 0, \quad \phi = \phi_{\mathrm{w}}, \tag{19}$$

$$\eta = 1: \ \frac{\partial u}{\partial \eta} = 0, \tag{20}$$

where the average value of the parameters can be calculated over the cross-section by

$$\langle \Gamma \rangle = \frac{1}{A} \int_0^1 \mathrm{d}A = \frac{1-\zeta}{1+\zeta} \int_0^1 (1-\eta) \Gamma \mathrm{d}\eta.$$

Then, the bulk mean dimensionless temperature u_{B}, the bulk mean dimensionless temperature θ_{B}, and the bulk mean nanoparticle volume fraction ϕ_{B} can be obtained as follows:

$$\begin{cases} u_{\mathrm{B}} = 2\dfrac{1-\zeta}{1+\zeta} \displaystyle\int_0^1 (1-\eta) u \mathrm{d}\eta, \\ \theta_{\mathrm{B}} = 2\dfrac{1-\zeta}{1+\zeta} \displaystyle\int_0^1 (1-\eta) \frac{\rho c u \theta}{\rho c u} \mathrm{d}\eta, \\ \phi_{\mathrm{B}} = 2\dfrac{1-\zeta}{1+\zeta} \displaystyle\int_0^1 (1-\eta) \frac{u \phi}{u} \mathrm{d}\eta. \end{cases} \tag{21}$$

The dimensionless heat transfer coefficient C_{htc} at the inner and the outer walls can be defined, respectively, by

$$C_{\mathrm{htc}i} = \frac{q_1 (R_2 - R_1)}{k_{\mathrm{bf}} (\theta_i - \theta_{\mathrm{B}})} = -\frac{\epsilon}{(1+\epsilon)\theta_{\mathrm{B}}}, \tag{22}$$

$$C_{\mathrm{htc0}} = \frac{q_2 (R_2 - R_1)}{k_{\mathrm{bf}} (\theta_0 - \theta_{\mathrm{B}})} = \frac{\epsilon}{(1+\epsilon)(\theta_0 - \theta_{\mathrm{B}})}. \tag{23}$$

The total heat transfer ratio can be expressed as

$$C_{\mathrm{htct}} = \frac{C_{\mathrm{htc0}} R_2 + C_{\mathrm{htc}i} R_1}{R_2 + R_1} = \frac{C_{\mathrm{htc0}} + C_{\mathrm{htc}i} \zeta}{1+\zeta}, \tag{24}$$

and the non-dimensional pressure drop can be defined by

$$N_{\mathrm{p}} = \frac{-(\mathrm{d}p/\mathrm{d}x)}{(\mu_{\mathrm{bf}} u_{\mathrm{B}})/(R_2 - R_1)^2} = \frac{\rho_{\mathrm{B}}}{\rho u}. \tag{25}$$

3 Application of HAM

In this paper, the HAM, which has been proved to be a strong and effective mathematical method to solve highly nonlinear problems, is employed to get the series solutions. For the analytical solution of Eqs. (16)–(20), using the HAM, we can select the following initial guess solutions:

$$u_0(\eta) = \eta - 0.5\eta^2, \quad \theta_0(\eta) = -\eta + \eta^2, \quad \phi_0(\eta) = \phi_{\mathrm{B}}. \tag{26}$$

The auxiliary linear operators are

$$L_u = \frac{\mathrm{d}^2 u}{\mathrm{d}\eta^2}, \quad L_\theta = \frac{\mathrm{d}^2 \theta}{\mathrm{d}\eta^2}, \quad L_\phi = \frac{\mathrm{d}\phi}{\mathrm{d}\eta}. \tag{27}$$

The properties satisfied by the auxiliary linear operator are

$$L_u(C_1 + C_2\eta + C_3\eta^2) = 0, \quad L_\theta(C_4 + C_5\eta + C_6\eta^2) = 0, \quad L_\phi(C_7 + C_8\eta) = 0, \tag{28}$$

where C_i $(i = 1, \cdots, 8)$ are constants.

The mth-order deformation equations are constructed as follows:

$$\begin{cases} L_u(u_m(\eta) - \chi_m u_{m-1}(\eta)) = qh_u R_m(\eta), \\ L_\theta(\theta_m(\eta) - \chi_m \theta_{m-1}(\eta)) = qh_\theta R_m(\eta), \\ L_\phi(\phi_m(\eta) - \chi_m \phi_{m-1}(\eta)) = qh_\phi(\eta) R_m(\eta). \end{cases} \tag{29}$$

4 Convergence of HAM solutions

Professor Liao[17] has pointed that the convergence rate of the approximation for the HAM solution strongly depends on the values of the auxiliary parameters h_u, h_θ, and h_ϕ. It is straightforward to choose the proper values of h_u, h_θ, and h_ϕ, which ensures that the solution series is convergent. Figures 1–3 give the respective valid ranges of h_u, h_θ, and h_ϕ, respectively. From the figures, we can see that the valid ranges are

$$-4 \leqslant h_u \leqslant 4, \quad -0.1 \leqslant h_\theta \leqslant 0.01, \quad -4 \leqslant h_\phi \leqslant 0.5.$$

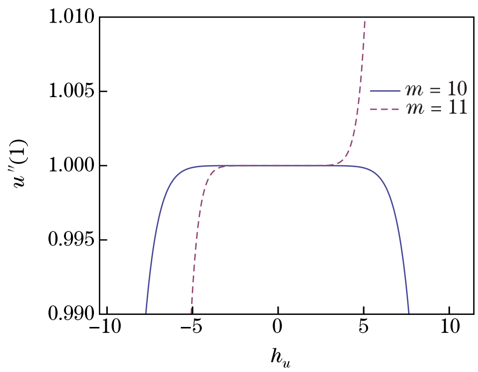

Fig. 1 h_u-curve of $u''(1)$

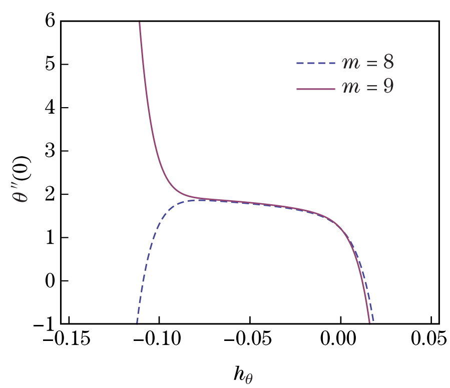

Fig. 2 h_θ-curve of $\theta''(0)$

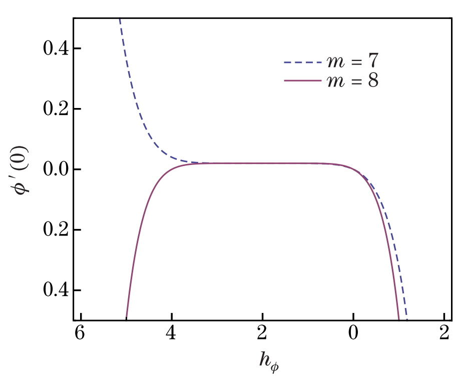

Fig. 3 h_ϕ-curve of $\phi'(0)$

Besides, We can use the residual error to find the proper h_u, h_θ, and h_ϕ. In this paper, we define the residual error $E_{m,\theta}^{[18]}$ by

$$E_{m,\theta} = \int_0^1 \Big((1-\eta)\Big(k\theta'' + k'\theta' - 2(1+\epsilon)\frac{k_{\mathrm{w}}}{q_{\mathrm{w}}}\frac{\rho c u}{\langle \rho c u\rangle} + Q_0\theta(1-\zeta)^2 + \frac{16\sigma^*}{3k^*}\theta''\Big) - k\theta'\Big)\mathrm{d}\eta. \tag{30}$$

Through following the square residual error function, Using BVPh2.0, the residual error in Fig. 4 shows that the higher the order of the HAM approximation is, the more accurate the result becomes. In addition, It can been seen that the present results agree well with those in Ref. [19] (see Table 1). Besides, the semi-analytical relation between Nu_{B} and N_{BT} can be obtained by

$$a = 2.149\,4(-4.589\,51\times10^{-5} - 4.055\,31\times10^{-7}N_{\mathrm{BT}} + 2.028\,5\times10^{-7}N_{\mathrm{BT}}^2 + 1.783\,01\times10^{-11}N_{\mathrm{BT}}^3), \tag{31}$$

$$b = -2.874\,01\times10^{-7}N_{\mathrm{BT}} + 1.439\,92\times10^{-7}N_{\mathrm{BT}}^2 + 1.506\,4\times10^{-11}N_{\mathrm{BT}}^3 + 2.337\,81\times10^{-17}N_{\mathrm{BT}}^4 - 2.080\,19\times10^{-5}, \tag{32}$$

$$c = 7.47(-1.689\,15\times10^{-2} + 1.713\,99\times10^{-2}N_{\mathrm{BT}} - 8.630\,23\times10^{-3}N_{\mathrm{BT}}^2) - 7.585\,78\times10^{-7}N_{\mathrm{BT}}^2)(-5.544\,67\times10^{-1} - 3.189\,53\times10^{-5}N_{\mathrm{BT}})^{-1} + 1, \tag{33}$$

$$Nu_{\mathrm{B}} = \frac{a}{bc}. \tag{34}$$

Table 1 Comparison of HAM results with results in Ref. [19]

ϕ_{B}	N_{BT}	$\rho C_p u\times10^{-4}$		N_{dp}		Nu_{B}	
		Ref. [19]	HAM	Ref. [19]	HAM	Ref. [19]	HAM
	0.5	10.280 40	10.286 52	108.108	107.070	5.030 96	5.037 00
0.06	1.0	10.491 50	10.491 83	142.857	143.222	5.128 21	5.143 00
	5.0	10.539 60	10.520 39	149.365	149.201	5.157 64	5.158 00

Figure 5 plots the semi-analytical relation between Nu_{B} and N_{BT}.

5 Results and discussion

For the Al-water nanofluid, when $d_{\mathrm{p}} \cong 10$ nm and $\phi_{\mathrm{B}} \cong 0.01$, the ratio of the Brownian motion to the thermophoretic forces $N_{\mathrm{BT}} \propto 1/d_{\mathrm{p}}$ ranges from 0.1 to 10. Moreover, when

$$\gamma = \frac{T_{\mathrm{w}} - T_{\mathrm{B}}}{T_{\mathrm{w}}} = 0.01,$$

its effects on the solution is negligible (see Ref. [8]). Hence, in the paper, the results are obtained for $\gamma = 0.01$. The effects of N_{BT}, λ_1, and λ_2 on the nanoparticle velocity u/u_{B}, the nanoparticle volume fraction ϕ/ϕ_{B}, the temperature profiles $\theta/\theta_{\mathrm{B}}$, the total heat transfer rate C_{htct}, and the pressure drop N_{p} are shown in Table 2 and Figs. 6–17. In these figures, $\eta = 1$ corresponds to the inner region of the microtube, whereas $\eta = 0$ corresponds to the outer region.

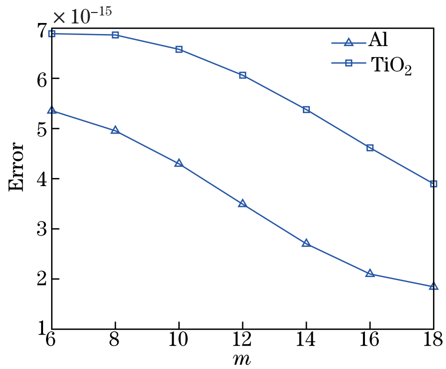

Fig. 4 Residual errors with HAM approximations order m in different nanofluids

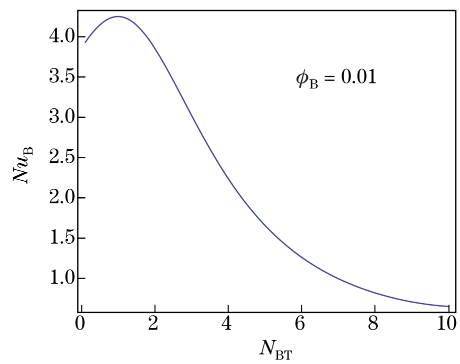

Fig. 5 Effects of N_{BT} on Nu_{B}

Table 2 Results of concentration gradient $|u'(0)|$

Ha	λ_2	λ_1	N_{BT}	ϵ	$\|u'(0)\|$	Ha	λ_2	λ_1	N_{BT}	ϵ	$\|u'(0)\|$
0	0.1	0.1	0.5	0.5	3.997 60	0	0.1	0.2	0.5	0.5	2.857 15
5	0.1	0.1	0.1	0.5	3.997 36	0	0.2	0.2	0.5	0.5	4.000 01
10	0.1	0.1	0.1	0.5	3.995 92	0	0.3	0.2	0.5	0.5	6.666 72
0	0.1	0.1	0.5	0.5	3.997 60	0	0.1	0.1	0.1	0.5	3.998 32
0	0.1	0.2	0.5	0.5	2.857 14	0	0.1	0.1	5.0	0.5	3.998 08
0	0.1	0.3	0.5	0.5	2.222 22	0	0.1	0.1	10.0	0.5	3.997 60

When nanoparticles migrate, the viscosity and thermal conductivity distributions are mainly decided by the mutual effects of the Brownian diffusion and the thermophoresis. The Brownian diffusion is proportional to the concentration gradient, while the thermophoresis is proportional to the temperature. From Table 2, we can see that the nanoparticles migrate from the heated wall towards the colder wall at lower values of N_{BT}. This is because that the migration reduces the viscosity and the shear stress. Considering Eqs. (5) and (6), the thermal conductivities of the nanoparticles strongly depend on the volume fraction. Therefore, when N_{BT} increases, the thermal conductivity of the heated wall and pressure drop increases, while the temperature gradient of the heated wall decreases (see Fig. 6). The nanoparticle concentration $\frac{\phi}{\phi_{\mathrm{B}}} \cong 1$ at the higher values of N_{BT} can be observed from Fig. 7, which means that it becomes uniform.

The slip parameters λ_1 and λ_2 mean the amount of the slip velocity at the surface. The effects of the first-order and second-order velocity slip parameters λ_1 and λ_2 on $\frac{u}{u_{\mathrm{B}}}$, $\frac{\theta}{\theta_{\mathrm{B}}}$, and $\frac{\phi}{\phi_{\mathrm{B}}}$ are shown in Figs. 8–13. Because the mass flow rate is assumed to be constant, the velocity in the core region must decrease if it increases at the wall due to the continuity law (see Fig. 8). Apparently, when λ_1 increases, the velocities increase near the outer wall while decrease markedly near the inter wall (see Fig. 8). Figure 9 shows that a steeper temperature gradient at the walls is obtained. From Fig. 10, we can see that, the nanoparticle volume fraction $\frac{\phi}{\phi_{\mathrm{B}}}$ has an increasing trend when λ_1 increases. From Fig. 11, we can see that, when λ_2 increases, the velocities increase. However, the temperature profile $\frac{\theta}{\theta_{\mathrm{B}}}$ and the nanoparticle volume fraction profile $\frac{\phi}{\phi_{\mathrm{B}}}$ show obvious differences when the second-order slip condition is considered (see Figs. 12 and 13). The exchanges of the momentum between the fluid layers lead to an increase in the heat transfer rate C_{htct} (see Fig. 14). However, an inverse trend can be observed for the pressure drop N_{p} (see Fig. 15). When λ_2 increases, both the nanoparticle volume fraction $\frac{\phi}{\phi_{\mathrm{B}}}$

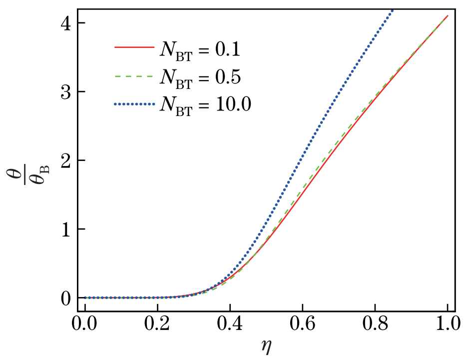

Fig. 6 Effects of N_{BT} on $\frac{\theta}{\theta_{\mathrm{B}}}$

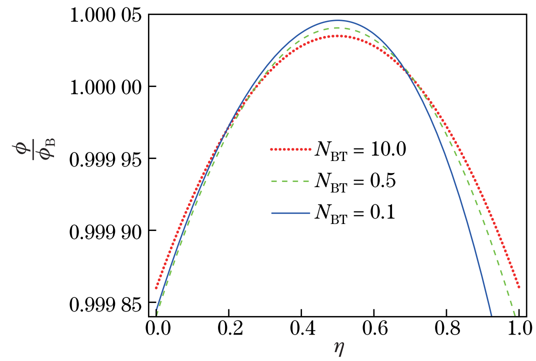

Fig. 7 Effects of N_{BT} on $\frac{\phi}{\phi_{\mathrm{B}}}$

and the pressure drop N_{p} increase (see Figs. 13 and 17). From Figs. 14–17, we can see that, no matter increasing λ_1 or λ_2, the heat transfer rate C_{htct} has an increasing trend, meanwhile, the pressure drop N_{p} has an inverse trend. Hence, λ_1 and λ_2 are positive parameters in the current heat transfer system.

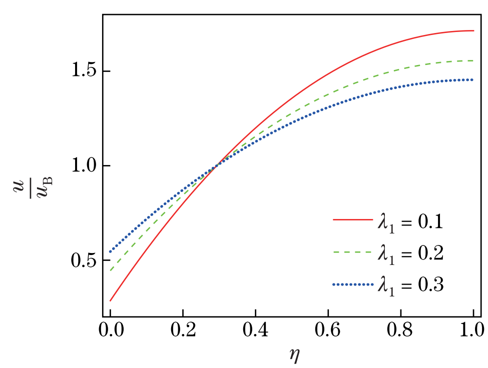

Fig. 8 Effects of λ_1 on $\frac{u}{u_{\mathrm{B}}}$

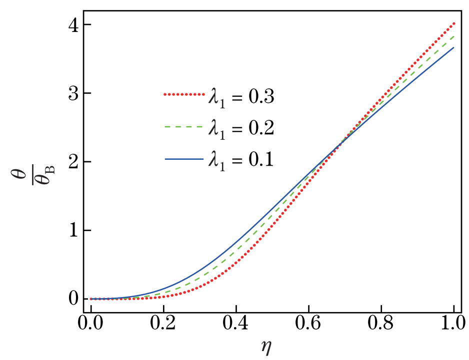

Fig. 9 Effects of λ_1 on $\frac{\theta}{\theta_{\mathrm{B}}}$

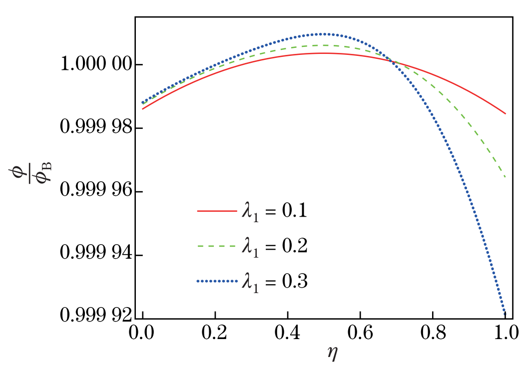

Fig. 10 Effects of λ_1 on $\frac{\phi}{\phi_{\mathrm{B}}}$

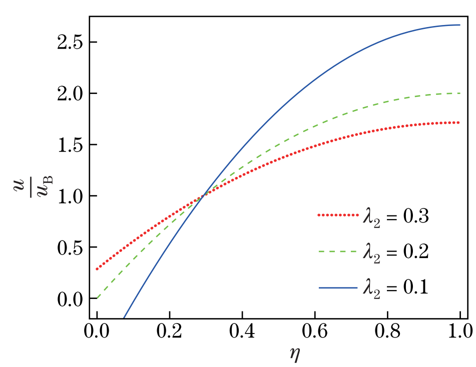

Fig. 11 Effects of λ_2 on $\frac{u}{u_{\mathrm{B}}}$

Figures 18 and 19 show the effects of the nanoparticles volume fraction ϕ_{B} on the heat transfer coefficient C_{htct} and the pressure drop N_{p} for a range of N_{BT}. From Eq. (5), we can see that increasing the bulk nanoparticle concentration leads to an increase in the viscosity with

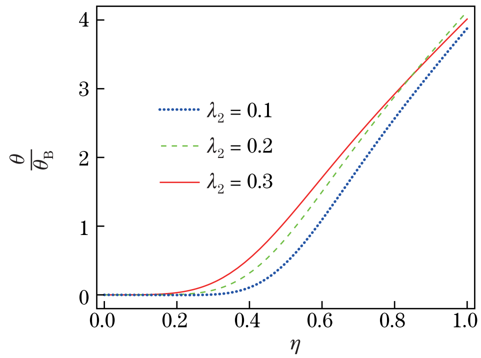

Fig. 12 Effects of λ_2 on $\frac{\theta}{\theta_B}$

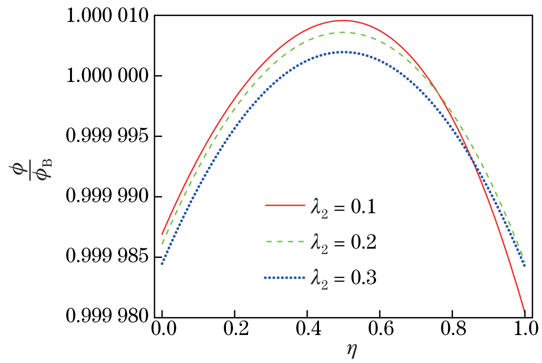

Fig. 13 Effects of λ_2 on $\frac{\phi}{\phi_B}$

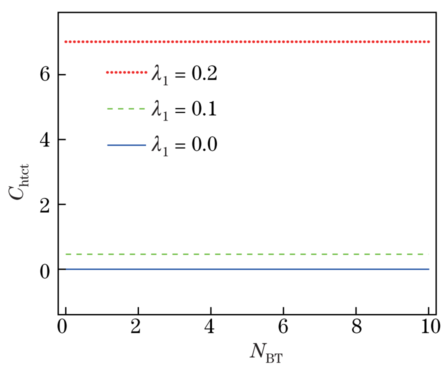

Fig. 14 Effects of λ_1 on C_{htct}

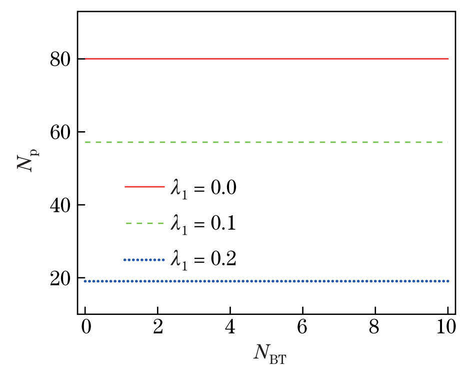

Fig. 15 Effects of λ_1 on N_{p}

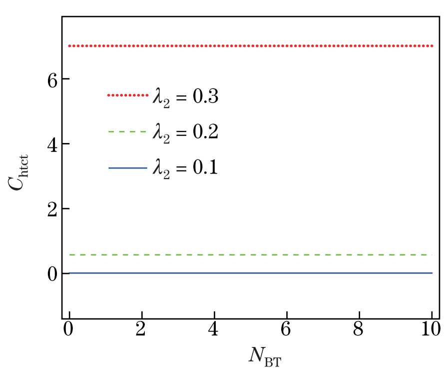

Fig. 16 Effects of λ_2 on C_{htct}

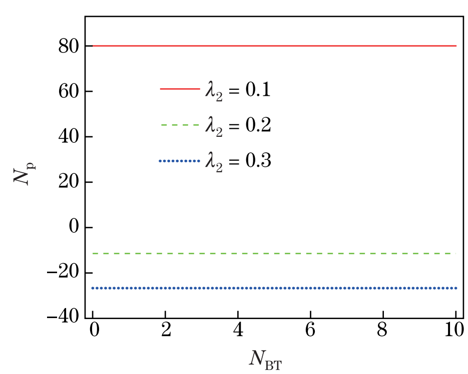

Fig. 17 Effects of λ_2 on N_{p}

nanoparticle concentration. Therefore, when the bulk nanoparticle concentration increases, the pressure drop along the channel increases obviously. From Fig. 19, we can see that the total heat transfer ratio increases when the nanoparticle volume fraction ϕ_{B} increases. Figure 19 depicts the heat transfer variation with different values of the nanoparticle volume fraction ϕ_{B}. When ϕ_{B} increases, since there are more suspended particles, the heat transfer coefficient increases because of the increasing viscosity at the walls, which suppresses the convection rate.

The Hartmann number Ha is the ratio of the electromagnetic force. Figures 20 and 21 depict the heat transfer coefficient C_{htct} and the pressure drop N_{p} versus N_{BT} for different values of Ha. Figure 20 depicts the heat transfer variation with different values of Ha. From the figure,

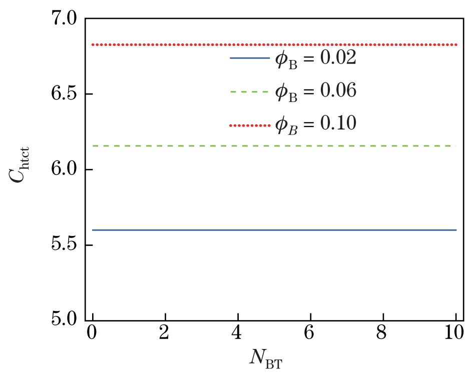

Fig. 18 Effects of ϕ_B on C_{htct}

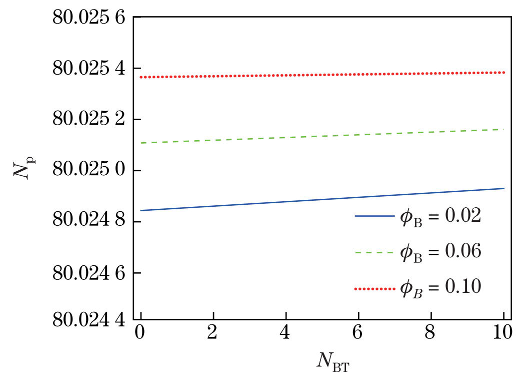

Fig. 19 Effects of ϕ_B on N_p

we can see that the total heat transfer ratio decreases when Ha increases, which means that in the presence of magnetic field, the advantage of nanofluids in heat transfer enhancement is reduced. An opposite phenomenon happens with an increase in Ha (see Fig. 21).

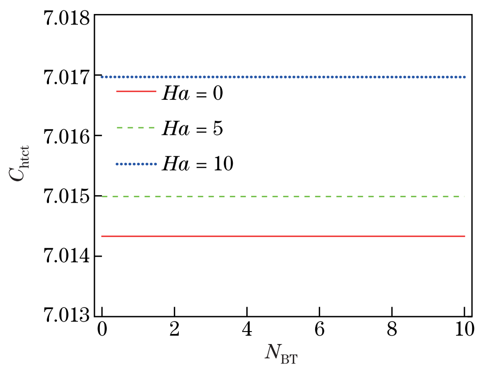

Fig. 20 Effects of Ha on C_{htct}

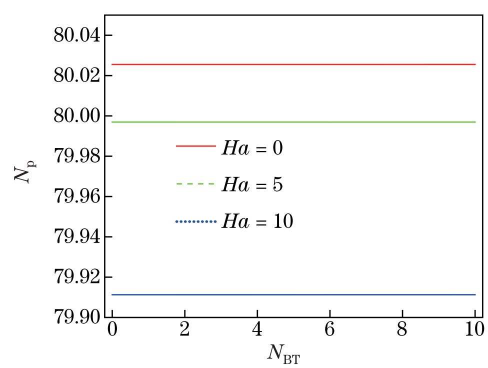

Fig. 21 Effects of Ha on N_p

6 Conclusions

In this paper, the second-order velocity slip on the MHD flow and heat transfer of the nanofluid in an annulus is studied by the HAM. The analytic solutions are obtained through the HAM. The major findings of this paper can be assorted as follows:

(i) It can be observed that the nanoparticle concentration in the annulus is progressively uniform when N_{BT} increases.

(ii) Both the one-slip parameter and the second-order slip parameter have positive effects on the total heat transfer rate and the pressure drop of the MHD flow.

(iii) The semi-analytical relation between Nu_B and N_{BT} is obtained.

(iv) Increasing ϕ_B increases the heat transfer coefficient C_{htct}.

References

[1] Wang, F. C. and Wu, H. A. Enhanced oil droplet detachment from solid surfaces in charged nanoparticle suspensions. *Soft Matter*, **9**, 7974–7980 (2013)

[2] Qin, X. C., Yuan, Q. Z., Zhao, Y. P., Xie, S. B., and Liu, Z. F. Measurement of the rate of water translocation through carbon nanotubes. *Nano Letters*, **11**, 2173–2177 (2011)

[3] Li, Y. Q., Wang, F. C., Liu, H., and Wu, H. A. Nanoparticle-tuned spreading behavior of nanofluid droplets on the solid substrate. *Microfluid Nanofluid*, **18**, 111–120 (2015)

[4] Yuan, Q. Z. and Zhao, Y. P. Precursor film in dynamic wetting, electrowetting, and electro-elasto-capillarity. *Physical Review Letters*, **104**, 1–4 (2010)

[5] Thompson, P. A. and Troian, S. M. A general boundary condition for liquid flow at solid surfaces. *nature*, **389**, 360–362 (1997)

[6] Wang, F. C. and Zhao, Y. P. Slip boundary conditions based on molecular kinetic theory: the critical shear stress and the energy dissipation at the liquid-solid interface. *Soft Matter*, **7**, 8628–8634 (2011)

[7] Wu, L. A. A slip model for rarefied gas flows at arbitrary Knudsen number. *Applied Physics Letters*, **93**, 1–3 (2008)

[8] Beskok, A. and Karniadakis, G. E. Rarefaction and compressibility effects in gas microflows. *Journal of Fluids Engineering*, **118**, 448–456 (1996)

[9] Zhu, J., Yang, D., Zheng, L. C., and Zhang, X. X. Effects of second order velocity slip and nanoparticles migration on flow of Buongiorno nanofluid. *Applied Mathematics Letters*, **52**, 183–191 (2016)

[10] Buongiorno, J. Convective transport in nanofluids. *Journal of Heat Transfer*, **128**, 240–250 (2006)

[11] Sheikholeslami, M., Vajravelu, K., and Rashidi, M. M. Forced convection heat transfer in a semi annulus under the influence of a variable magnetic field. *International Journal of Heat and Mass Transfer*, **92**, 339–348 (2016)

[12] Kasaeipoor, A., Ghasemi, B., and Aminossadati, S. M. Convection of Cu-water nanofluid in a vented T-shaped cavity in the presence of magnetic field. *International Journal of Thermal Sciences*, **94**, 50–60 (2015)

[13] Asad, S., Alsaedi, A., and Hayat, T. Flow of couple stress fluid with variable thermal conductivity. *Applied Mathematics and Mechanics* (*English Edition*), **37**(3), 315–324 (2016) DOI 10.1007/s10483-016-2031-6

[14] Hassan, H. and Harmand, S. Effect of using nanofluids on the performance of rotating heat pipe. *Applied Mathematical Modelling*, **39**, 4445–4462 (2015)

[15] Pak, B. C. and Cho, Y. I. Hydrodynamic and heat transfer studyof dispersed fluids with submicron metallic oxide particles. *Experimental Heat Transfer*, **11**, 151–170 (1998)

[16] Hakeem, A. K. A. and Sathiyanathan, K. An analytic solution of an oscillatory flow through a porous medium with radiation effect. *Nonlinear Analysis*: *Hybrid Systems*, **3**, 288–295 (2009)

[17] Liao, S. J. On the homotopy analysis method for nonlinear problems. *Applied Mathematics and Computation*, **147**, 499–513 (2004)

[18] Fan, T. *Applications of Homotopy Analysis Method in Boundary Layer Flow and Nanofluid Flow Problems*(in Chinese), Ph. D. dissertation, Shanghai Jiao Tong University, Shanghai (2012)

[19] Malvandi, A. and Ganji, D. D. Brownian motion and thermophoresis effects on slip flow of alumina/water nanofluid inside a circular microchannel in the presence of a magnetic field. *International Journal of Thermal Sciences*, **84**, 196–206 (2014)